
Kuro Siwo: 33 billion m^2 under the water

A global multi-temporal satellite dataset for rapid flood mapping

Nikolaos Ioannis Bountos^{1,2*}
bountos@noa.gr

Maria Sdraka^{1,2*}
masdra@noa.gr

Angelos Zavras^{1,2}
azabras@noa.gr

Ilektra Karasante¹
ile.karasante@noa.gr

Andreas Karavias¹
karavias@hua.gr

Themistocles Herekakis¹
therekak@noa.gr

Angeliki Thanasou¹
thanasou@gmail.com

Dimitrios Michail²
michail@hua.gr

Ioannis Papoutsis¹
ipapoutsis@noa.gr

¹ **Orion Lab**

National Observatory of Athens & National Technical University of Athens

² **Harokopio University of Athens**

Abstract

Global flash floods, exacerbated by climate change, pose severe threats to human life, infrastructure, and the environment. Recent catastrophic events in Pakistan and New Zealand underscore the urgent need for precise flood mapping to guide restoration efforts, understand vulnerabilities, and prepare for future occurrences. While Synthetic Aperture Radar (SAR) remote sensing offers day-and-night, all-weather imaging capabilities, its application in deep learning for flood segmentation is limited by the lack of large annotated datasets. To address this, we introduce Kuro Siwo, a manually annotated multi-temporal dataset, spanning 43 flood events globally. Our dataset maps more than 338 billion m^2 of land, with 33 billion designated as either flooded areas or permanent water bodies. Kuro Siwo includes a highly processed product optimized for flash flood mapping based on SAR Ground Range Detected, and a primal SAR Single Look Complex product with minimal preprocessing, designed to promote research on the exploitation of both the phase and amplitude information and to offer maximum flexibility for downstream task preprocessing. To leverage advances in large scale self-supervised pretraining methods for remote sensing data, we augment Kuro Siwo with a large unlabeled set of SAR samples. Finally, we provide an extensive benchmark, namely BlackBench, offering strong baselines for a diverse set of flood events globally. All data and code are published in our Github repository: <https://github.com/Orion-AI-Lab/KuroSiwo>.

1 Introduction

There is compelling evidence of compound effects that link extreme natural disasters worldwide [66]. The Intergovernmental Panel on Climate Change (IPCC) [72] underscores that floods represent

*Equal contribution

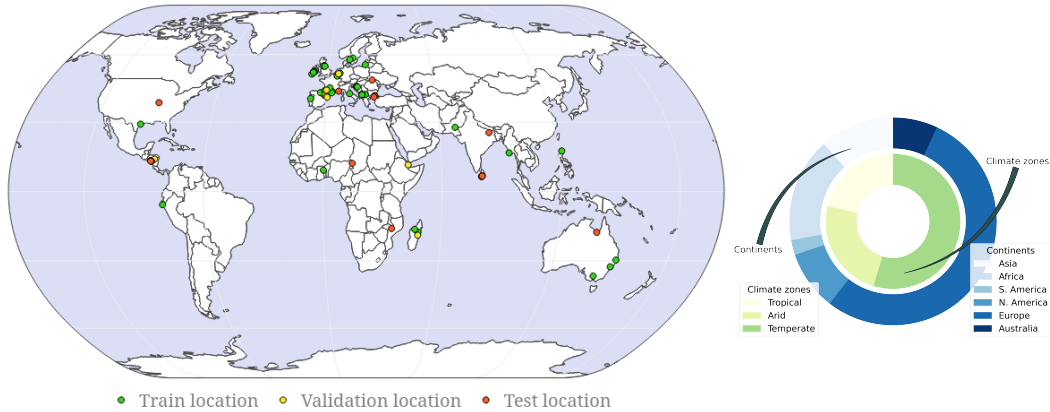


Figure 1: Spatial distribution of Kuro Siwo events. The test dataset encompasses flood events from entirely unseen locations on Earth.

the most frequent natural hazard globally and are projected to increase in frequency and intensity due to global warming [50, 6, 68]. The causes of flash floods, and more significantly, their expected impacts, exhibit significant variations contingent upon the exposure potential and vulnerabilities inherent in the affected population [77, 37] and socio-environmental assets [54]. In fact, floods tend to disproportionately affect the most impoverished and vulnerable segments of our society [67, 70, 11]. Research has revealed that approximately 170 million individuals exposed to substantial flood hazards are struggling with extreme poverty [67].

Recent tragic incidents in Pakistan [81, 82] and New Zealand [28] exemplify the gravity of flash floods, resulting in significant human casualties and substantial economic losses. According to the World Bank [83], the latest flood in Pakistan affected a staggering 33 million people, resulting in over 1,739 fatalities. The mismanagement of disasters triggered by floods in itself carries substantial risks. For instance, stagnant floodwaters, which present a significant hazard for the transmission of water-borne and vector-borne diseases, have left more than 8 million people in a state of health crisis [83] with over 4 million children still living near contaminated floodwaters [81].

Remote sensing (RS) provides an opportunity for systematic, rapid and accurate flood mapping [14], crucial for effective flood impact management. Accurate flood mapping streamlines disaster response and relief efforts, allowing emergency responders, humanitarian organizations, and government agencies to efficiently allocate resources, deliver aid, and support affected populations [36]. It plays a crucial role in safeguarding critical infrastructure by identifying vulnerable assets [53] and assists in assessing flood risks, guiding urban planning [23], land-use zoning [61, 80], and formulating flood mitigation strategies [42]. Accurate flood maps are indispensable for insurance companies and financial institutions in evaluating flood-related risks, and managing financial exposure [76, 52, 78]. In the face of intensifying climate change impacts, flood mapping is crucial for adapting to evolving environmental conditions [55]. Lastly, it contributes to scientific research, enhancing our understanding of flood dynamics [49] and facilitating more informed decision-making in the long run [5, 19].

The exploitation of satellite data for flood mapping has seen extensive use [10], particularly with the emergence of Sentinel satellite platforms [79]. Specifically, the Sentinel-2 multispectral and Sentinel-1 Synthetic Aperture Radar (SAR) missions offer global, detailed and frequent imaging of the Earth's surface. However, high precipitation and extensive cloud cover during flood events impact multispectral sensors which effectively become blind and unreliable for operational scenarios. In contrast, SAR operates seamlessly day and night, unaffected by weather conditions, making it better suited for operational flood mapping. Thus, our research focuses on developing methods that can rapidly map flooded areas using SAR data.

Modern computer vision methods have already shown great promise in multiple RS applications [74, 75, 9, 62]. However, to the best of our knowledge, no machine learning method has notably excelled in both robust performance and generalization across diverse global flood events. We identify two primary reasons for this. Firstly, the task is inherently complex due to the presence of speckle noise in SAR [43], manifesting as random brightness variations in backscatter imagery. Second, deep

Table 1: Public datasets for flood mapping. S1 stands for Sentinel-1, S2 for Sentinel-2, GF2 for GaoFen-2, GF3 for GaoFen-3, UAV for Unmanned Aerial Vehicle, DEM for Digital Elevation Model and OSMh for Openstreet Map hydrography. Annotation methods are abbreviated as follows: A - Automatic, SA - Semi-automatic, M - Manual, CEMS - Copernicus Emergency Management Service. We assume the 7 continent scheme.

Dataset	Sources	Imagery included?	SLC	GSD	# samples	sample size	# events	# events in test set	Timestamps	# continents	# classes	Annotation method
UNOSAT [60]	S1	✓	✗	10m	58,128	256x256	15	all + 1 new	Post	2	2	SA
SEN12-FLOOD [65]	S1, S2	✓	✗	10m	336	512x512	-	-	Time series	3	2	CEMS
Sen1Floods11 [8]	S1, S2	✓	✗	10m	4,831	512x512	11	1	Post	5	3	M, A
Ombria [22]	S1, S2	✓	✗	10m	1,688	256x256	23	all	Pre, Post	5	2	CEMS
WorldFloods [51]	S2	✓	✗	10m	185,574	256x256	119	6	Post	6	3	SA
GF-FloodNet [91]	GF2, GF3	✓	✗	1.5 - 5m	13,388	256x256	8	all + 3 new	Post	4	2	SA
Global Flood Database [77]	MODIS	✗	✗	250m	12,719	-	913	-	Post	6	2	A
SIGFloods [71]	S1	✓	✗	-	5,360	256x256	46	all + 2 new	Pre, Post	6	2	SA
MMFlood [56]	S1, DEM, OSMh	✓	-	20m	1,748	2000x2000	95	34	Post	6	2	CEMS
RAPID-NRT [89]	S1	✗	✗	10m	559	-	4	-	-	1	2	A
CAU-Flood [31]	S1, S2	✓	✗	10m	18,302	256x256	18	2	Pre, Post	4	2	M
FloodNet [64]	UAV	✓	-	1.5cm	2,343	4000x3000	1	1	Post	1	9	SA
ETCI2021 [59]	S1	✓	✗	20m	66,810	256x256	5	2	Post	3	2	-
Kuro Siwo (labelled)	S1, DEM	✓	✓	10m	67,490	224x224	43	10	2 Pre, Post	6	3	M
Kuro Siwo (unlabelled)	S1, DEM	✓	✓	10m	466,357	224x224	43	10	2 Pre, Post	6	3	M

learning methods require a substantial amount of well-curated training data to fulfill their potential. While the Sentinel-1 mission offers abundant data for leveraging these methods in flood mapping, a comprehensive and well-annotated dataset is currently absent. This phenomenon is magnified when considering both the phase and amplitude information of SAR data.

To overcome this barrier, we curate time series data from Sentinel-1 SAR imagery linked to flood events worldwide, and manually annotate them with the expertise of SAR specialists. We provide two SAR products paired with the resulting reference annotation maps: Ground Range Detected (GRD) SAR with preprocessing tailored for flood mapping and Single Look Complex (SLC) SAR data with minimal preprocessing, containing both phase and amplitude signal. Additionally, we incorporate unlabeled SAR samples, to facilitate the exploration of semi-supervised and large-scale self-supervised learning (SSL). We name the resulting dataset “Kuro Siwo”² and release it publicly with the aim to propel research in this field towards developing operational tools that support civil protection authorities for the greater good.

Our main contributions can be summarized as follows:

- We publish Kuro Siwo, a global, manually annotated multi-temporal SAR dataset providing labels for 43 distinct flood events. Kuro Siwo consists of time series SAR imagery with dual polarization paired with elevation information. Its sheer size, meticulous annotation process and diversity make it a unique and highly valuable dataset for rapid flood mapping.
- Kuro Siwo is the first flood mapping dataset to provide both and coregistered GRD and SLC SAR data, offering the opportunity to leverage both amplitude and phase information.
- We enhance Kuro Siwo with a large unlabeled SAR dataset, facilitating global representation learning alongside a well-defined downstream task for evaluation. The final dataset contains more than 1.6 million SAR images grouped into more than 533,000 time series.
- We publish the first benchmark on Kuro Siwo, namely BlackBench, offering diverse and strong baselines. BlackBench demonstrates the quality of Kuro Siwo, enabling the training of models that achieve performance higher than 80%, 78% and 83% F1-Score for flood, permanent and general water detection respectively on a challenging and diverse test set.

2 Related Work

2.1 Flood mapping datasets

In this section we summarize previous work on the creation of analysis-ready satellite based datasets for flood mapping. Our investigation is focused on three key aspects. First, the provided satellite sensors, second the ground truth generation process and finally the evaluation scheme. Please refer to Tab. 1 for an overview of our analysis.

²Named after a poem by sailor-poet Nikos Kavvadias (1910-1975).

Several datasets, such as SEN12-FLOOD, Sen1Floods11, Ombria, GF-FloodNet and CAU-Flood provide aligned multisource satellite imagery, facilitating the utilization of multiple modalities. A great number of datasets like UNOSAT, Sen1Floods11, WorldFloods, GF-FloodNet, MMFlood, ETCI2021 and FloodNet provide solely the post-flood acquisition omitting pre-event information which could greatly assist the mapping process and alleviate false positive predictions on permanent water bodies. In addition, databases like the Global Flood Database and RAPID-NRT comprise only flood mappings with no corresponding input imagery.

Given the difficulty and cost of satellite imagery photointerpretation, the creation of ground truth masks for large-scale datasets is not trivial, with many works offering automatic or semi-automatic methods to alleviate the need for a laborious labelling process (Tab. 1). Some datasets, like the Global Flood Database and RAPID-NRT, employ automatic annotation methods, introducing noise and inaccuracies in the labels due to their reliance on input data quality. Others, such as UNOSAT, WorldFloods, GF-FloodNet, SIGFloods, and FloodNet, utilize a semi-automatic pipeline where automatically generated labels undergo refinement by human annotators. It's worth noting that in Sen1Floods11, only 446 samples from a single event were manually annotated, while the rest used a thresholding method without human intervention. Manual labeling through meticulous photointerpretation produces higher-quality ground truth mappings. Nevertheless, this approach is expensive, requiring expert input and potentially introducing annotator bias. Such labels have been produced for the CAU-Flood dataset to generate binary flood/no flood masks.

The proposed evaluation scheme is crucial for assessing the generalization capabilities of any flood mapping method. However, in Sen1Floods11, WorldFloods, CAU-Flood, ETCI2021 and FloodNet, a limited number of events are reserved for testing, potentially providing an insufficient indicator of a model's performance on unseen conditions. Additionally, in UNOSAT, Ombria, GF-FloodNet, and SIGFloods, samples from all flood events are shuffled and randomly split into training, validation, and test sets, posing a risk of data leakage where samples from the same area and satellite capture may appear in both training and test sets. To address this concern, the authors of UNOSAT, GF-FloodNet, and SIGFloods have also performed evaluation on imagery from a small number of new, unseen flood events, though these events are not included in the published datasets.

To our knowledge Kuro Siwo is the first flood mapping dataset offering ground truth labels based on expert photointerpretation at such an unprecedented scale (43 events), with wide spatial coverage spanning 6 out of 7 continents and 3 out of 4 major climate zones. Kuro Siwo can be the first step towards unlocking the true potential of deep learning methods for rapid flood mapping.

It is worth noting that phase information of SAR imagery has been consistently overlooked by the community regardless of the application. However, the phase signal can be used to generate useful byproducts, such as interferometric coherence that is suited for change detection applications [57] and especially for flood mapping [63]. In fact, S1SLC_CVDL [2] and OpenSarShip2.0 [44] are, to our knowledge, the only existing substantial datasets offering SLC data, both addressing tasks unrelated to floods. Kuro Siwo stands out as the only large-scale dataset that not only offers time series of SLC data paired with high-quality annotations but also provides wide spatiotemporal coverage with 43 flood events from 2015 till 2022.

2.2 Deep learning for rapid flood mapping from SAR imagery

Several studies have explored the synergistic use of SAR and multispectral imagery, aiming to capitalize on the strengths of both modalities. In works such as [65] and [22], simple CNN models extract features from a time series of both modalities, concurrently leveraging spatial and temporal contexts. In [33] the authors investigate domain adaptation techniques applied to various machine learning algorithms. Notably, [3, 58, 92] focus on post-flood imagery and experiment with CNN architectures distinguishing flood water from permanent water, assisted by auxiliary DEM input. Transfer learning approaches between SAR and multispectral domains have been explored in works like [46], [39], and [26], whereas in [31] a U-Net-like architecture with transformer modules is trained on Sentinel-2 pre-flood and Sentinel-1 post-flood images.

Nevertheless, multiple studies have focused solely on the use of SAR imagery due to its all weather imaging capabilities, and have designed various CNN architectures in order to segment the post-flood SAR image into flooded/non-flooded pixels (e.g. [38], [60], [85], [86], [13], [35], [1]). On the other hand, a number of methods opt for bitemporal imagery as input to their models in order to perform

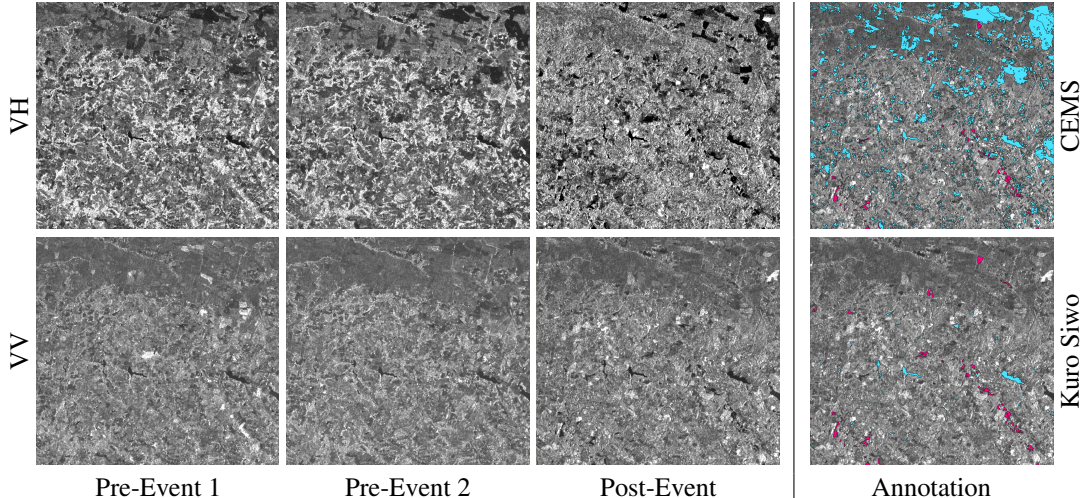


Figure 2: (left) Mosaic depicting Kuro Siwo samples for both VV and VH polarizations. (right) Copernicus Emergency Management Service (CEMS) annotations for a 2020 flood event in an agricultural area in France vis à vis Kuro Siwo photointerpretation. Cyan denotes permanent water bodies while purple indicates flooded areas. Notably, errors in CEMS annotations are apparent, particularly in the permanent waters class, suggesting the possibility that the CEMS annotator solely relied on VH polarization for annotation in this particular example. Quantitatively, the two products exhibit IoU of 51% and 48% for the permanent water and flood categories respectively.

change detection analysis and better isolate the flooding events. For example, [34] utilize simple dual-branch CNN architectures on bitemporal SAR data, whereas [20], [90] and [71] exploit transformer networks for better feature and context extraction. In [93] a dual-branch CNN is pretrained on water extraction and then finetuned on flood inundation mapping, while in [27] a sparse autoencoder is employed for the creation of pseudo-labels which are then used to train a simple small CNN. Finally, in [84] the model is also assisted by salient maps produced using the backscatter coefficient, and in [88] a time series of pre-flood SAR acquisitions is fed as input to a U-Net with ConvLSTM modules which is trained in a contrastive self-supervised way.

3 Kuro Siwo dataset

Requirements: While substantial efforts have been invested in automated flood mapping, the absence of a diverse and well-curated remote sensing dataset hampers the potential of deep learning methods for this critical task. To address this gap, we present Kuro Siwo, a distinctive flood inundation mapping dataset constructed with specific constraints. Firstly, the dataset is SAR-based, ensuring availability of usable imagery in all weather conditions, day and night, even during production in an operational context. In addition, we stick to SAR imagery from the Sentinel-1A&B satellites, since Copernicus data are available on a free and open basis, and there is strong commitment for the continuity of the mission. Secondly, Kuro Siwo is designed as a multi-temporal dataset to enable distinguishing between permanent water bodies, e.g rivers and lakes, and flooded areas, and also to facilitate testing change detection computer vision architectures. Thirdly, Kuro Siwo aims for diversity, featuring extensive spatio-temporal coverage of 43 major flood events spanning from 2015 to 2022, across six continents and three climate zones. The omission of flood events in Antarctica and polar/cold climate zones reflects their real-life distribution, as these areas typically do not experience floods. Fig. 1 illustrates the spatial coverage of Kuro Siwo, including the distribution of climate zones. Lastly, we prioritize the generation of high-quality flood annotations at a global scale, achieved through manual photointerpretation by a group of SAR experts, surpassing those from existing sources like the Copernicus Emergency Management Service (CEMS).

Input data: For each event, we assemble a triplet of Sentinel-1 data at two forms: a) Level-1 GRD SAR data and b) Level-1 SLC SAR data, both at 10 m spatial resolution. This triplet comprises two pre-event images with varying temporal distances — eliminating rigid constraints for real-world applications — and one post-event image acquired as close as possible to the actual event date. The

temporal gap depends on the sensor revisit time and the location on earth, resulting in a mean of 3.6 days (with std of 6.07 days) and a median of 1 day in post-event captions. We impose that for each flood event, all three SAR images belong to either the descending or ascending imaging geometry to prevent variations in layover, foreshortening and shadow effects [16] within the same sample. Additionally, for each SAR image in Kuro Siwo, both VV (Vertical transmit and Vertical receive) and VH (Vertical transmit and Horizontal receive) polarizations are registered, as studies have demonstrated their complementary value for flood mapping [45, 32].

GRD Preprocessing: To prepare our data for deep learning methods, we employ a standard Sentinel-1 GRD preprocessing pipeline [25] through the Sentinel Application Platform (SNAP) [95]. This pipeline involves precise orbit application, removal of thermal and border noise, land and sea masking, calibration, speckle filtering and terrain correction using an external digital elevation model (DEM), i.e. SRTM 1 Sec. The output of this pipeline yields a radiometrically calibrated SAR backscatter.

SLC preprocessing: Furthermore, we develop a minimal preprocessing pipeline for the SAR SLC data with two goals: a) create a foundation dataset of unrefined georeferenced SLC SAR data paired with quality annotations, allowing the end user to make all subsequent processing decisions, and b) provide the first baseline models utilizing complex valued input with both the phase and amplitude information on Kuro Siwo. Our processing pipeline includes swath selection, precise orbit application and debursting. We then extract the phase and amplitude information from the complex data and apply terrain correction using an external DEM (SRTM 1 Sec).

Dataset creation: The events included in Kuro Siwo can be split in two categories: a) events that have been previously annotated by the CEMS and b) events without any publicly available annotation. When CEMS annotations are available, we initialize the labeling process by utilizing the original CEMS shapefiles; otherwise we begin from scratch. Subsequently, we engage, with a team of five SAR experts, in the photointerpretation of the GRD preprocessed images and generate the ground truth masks assigning each pixel to one of three categories, i.e. Permanent Waters, Floods and No Water. The detailed annotation procedure and principles can be found in the Supplemental Material. The resulting flood mapping dataset contains 67,490 timeseries with 202,470 unique SAR samples stored as 224×224 tiles, along with all necessary metadata including the caption dates, the respective climate zone, the id of the area of interest, the Digital Elevation Model (obtained from SRTM 1Sec) etc. We provide both GRD and the SLC processed products for all events, along with deep learning ready time series-reference maps pairs. Kuro Siwo is released under the MIT License.³

Why update CEMS annotations? Some existing datasets used for rapid flood mapping with Sentinel-1 SAR data rely on the freely available CEMS annotations, which cover a large number of events globally. Typically, these annotations involve a combined thresholding and photointerpretation approach during a CEMS Activation. There are three significant challenges associated with CEMS annotations. Firstly, these Activations require the delivery of flood delineation products within an exceptionally short time frame, usually a few hours upon receiving the satellite imagery, leading to human errors in the annotations. Secondly, different teams within Copernicus annotate various flood events, resulting in variable photointerpretation and methodological biases in the annotations. Lastly, quality standards requirements have evolved in CEMS over the years, and consequently, the latest flood activations provide better quality annotations compared to older ones.

The above result in problematic annotations that hamper the potential to train robust and accurate deep learning models. For example, the creators of the Ombria [22] and the MMFlood [56] datasets (Tab. 1) that both use CEMS annotations, report low classification accuracies. This was our experience also when we used the original CEMS annotations; our deep learning models achieved less than 70% for all evaluation metrics. Therefore we decided to invest in updating CEMS annotations through photointerpretation. Fig. 2 exemplifies the annotation improvement attained in Kuro Siwo for a flood event in an agricultural area in France. The errors in CEMS annotations, especially for the permanent waters class, are obvious when carefully examining both polarizations. To discern the disparity between the CEMS and Kuro Siwo annotation for the specific flood event, the two products exhibit Intersection over Union (IoU) of 51% and 48% for the permanent water and flood categories, respectively.

Going beyond CEMS: Building on CEMS annotations, which focuses primarily on Europe, results in severe underrepresentation of other continents. Recognizing this, we expand our study on flood

³<https://opensource.org/license/MIT>

events from Asia, Australia, Africa as well as South and North America, aiming for a more balanced spatial distribution. These events cover extensive areas providing a substantial number of additional training patches. Floods in Europe are fragmented small scale events, as opposed to large flood events encountered in other continents, e.g. Asia. Consequently, while most events in Kuro Siwo are from Europe compared to Asia, the latter contributes with more samples.

Dataset split: Scholastically assessing and comparing the capacity of flood mapping models to operate in novel environments is of great importance to reliably evaluate future methods and eventually deploy them in the real world. With that in mind, we construct a challenging evaluation framework, selecting 10 flood events across the globe as testing sites, covering a wide range of environmental conditions representing all six continents and three major climate zones featured in Kuro Siwo. The spatial distribution of training, validation and test flood events in Kuro Siwo is illustrated in Fig. 1 along with the continents representation.

Unlabeled component: In the context of natural hazards and extreme events, instances of positive occurrences, such as floods, volcanic unrest [9], landslides [7] and wildfires [41], are notably rare. This scarcity results in a limited dataset, insufficient for mapping the diverse, intricate and dynamic environmental variables, including water. Furthermore, the number of flash floods monitored with publicly available SAR imagery is finite, given that Sentinel-1 data are available after 2014 only, while at the same time, acquiring and photointerpreting them all implies a substantial cost. Recognizing these constraints and the importance of generalizing to unseen events, we offer an extensive, unlabeled collection of satellite frame triplets, adhering to the same principles and preprocessing pipeline as the annotated Kuro Siwo set. This resultant dataset encompasses 533,847 time series with 1,601,511 unique SAR samples. Motivated by recent advancements in foundational models for computer vision [40], we release this dataset to encourage the exploration of SSL methods specifically designed for the domain of rapid flood mapping.

4 BlackBench: An extensive benchmark on rapid flood mapping

Building on Kuro Siwo, we introduce BlackBench, an extensive benchmark employing a large set of powerful models under various configurations to act as strong baselines for future methods. BlackBench includes common semantic segmentation architectures like U-Net [69], DeepLabv3 [12] and UPerNet [87] using both convolutional and transformer backbones like the ResNet [30] family, Swin Transformer [47] and ConvNext [48]. We use two variants of each backbone for UPerNet indicated as Small (S) and Base (B) as defined in [15]. Furthermore, we include a set of models inspired by change detection problems, like FC-EF-Diff and FC-EF-Conc [17], which were among the first deep learning models proposed for this task. Additionally, we include SNUNet-CD [24], a densely connected U-Net++ [94] model with a dual-branch encoder, and Changeformer [4], a model consisting of two siamese branches with transformer blocks and a lightweight MLP decoder. Finally, we explore ConvLSTM [73], a recurrent convolutional architecture suitable for time-series data. We employ an encoder-decoder architecture, and we select only the last output map for an N-to-1 scheme.

For each model included in BlackBench, we assess the performance across diverse input scenarios, using GRD data. The input setting varies on two factors. First, in regard to the time series length and second, in regard to the inclusion of elevation information. For all semantic segmentation models we consider time series of either 2 or 3 images varying the number of pre-event captions. For the change detection models we strictly use two captions by selecting only the most recent pre-flood image since this family of architectures typically employs a two-stream input encoder. For each time series length, we examine the performance of the models when we a) include a DEM, b) include slope information (derived from the DEM) and c) provide no elevation information at all. In Tab. 2 we report the performance of the best setting for each architecture. In particular, we report the F1-Score (F1) for each class as well as the overall mean IoU (mIoU). Additionally, we evaluate the F1-Score for the binary task of water detection by combining the predictions for permanent water and flood into one “water” class. All semantic segmentation models use pretrained backbones and were trained for 20 epochs. U-Net and DeepLabv3 models use backbones pretrained on ImageNet [18], while UPerNet uses backbones from [15]. Change detection and recurrent models were trained from scratch for 150 epochs. Finally, we create a baseline model trained via SSL using the unlabeled component of Kuro Siwo, excluding the events from the test set. To model interactions in the temporal dimension as well as make the finetuning process more direct, we treat each Kuro Siwo triplet as one sample. We utilize the Masked Autoencoder [29] (MAE) method employing a vision transformer [21] (ViT) with 24

Table 2: This table presents the best performing setting for each architecture utilising the GRD data, in regards to the time series length as well as the utilization of elevation information. “No water”, “permanent water”, “flood” and “water” classes are represented by NW, PW, F and W respectively. Best values are marked in **bold**, second best are underlined.

Model	Caps.	DEM	Slope	F1-NW(%)	F1-PW(%)	F1-F(%)	mIOU(%)	F1-W(%)
UNet-ResNet18	2	-	-	98.72	76.01	<u>79.86</u>	75.12	83.31
UNet-ResNet50	3	-	-	<u>98.73</u>	<u>78.24</u>	80.12	76.20	83.85
UNet-ResNet101	3	-	✓	<u>98.69</u>	79.33	78.92	<u>76.12</u>	82.88
DeepLab-ResNet18	3	-	✓	98.74	77.35	78.51	75.07	83.38
DeepLab-ResNet50	3	-	✓	98.71	77.35	78.70	75.14	83.20
DeepLab-ResNet101	2	-	-	98.65	77.03	78.46	74.84	82.52
UPerNet-SwinS	2	-	✓	98.70	77.59	78.95	75.35	82.51
UPerNet-SwinB	3	-	-	98.72	76.94	79.28	75.22	83.15
UPerNet-ConvnextS	3	-	-	98.65	77.09	79.3	75.26	82.86
UPerNet-ConvnextB	2	-	-	98.60	77.00	78.15	74.66	82.57
FloodViT	3	-	-	<u>98.73</u>	75.23	78.70	74.22	83.21
FloodViT-FT	3	-	-	98.74	75.45	78.35	74.17	83.03
FC-EF-Diff	2	✓	-	97.8	10.93	74.27	53.52	62.6
FC-EF-Conc	2	✓	-	98.64	71.89	75.06	71.17	82.04
SNUNet-CD	2	-	-	98.57	73.14	74.26	71.3	81.51
Changeformer	2	-	-	98.66	74.84	76.96	73.23	82.23
ConvLSTM	3	-	-	98.66	76.57	77.53	74.23	81.96

layers and 16 attention heads as our encoder and train for 100 epochs. We stack the triplets on the channel dimension as done with all segmentation methods in BlackBench. To model the varying temporal distances between the pre-event and the post-event captions, we include three temporal embeddings, i.e. one for each timestep. We encode the year, month and day independently using a sinusoidal encoding and concatenate them. The resulting temporal embeddings are added to the tokens as done with the standard, learnable positional embeddings. For the segmentation downstream task, we add a simple, trainable, convolutional decoder on top of the learnt representations. We evaluate the capacity of our model by a) keeping the encoder frozen and training only the decoder module, and b) finetune the last 12 transformer layers along with the decoder. We will refer to these models as FloodViT and FloodViT-FT respectively. We discuss the insights gained from BlackBench in detail in Sec. 5. Furthermore, we provide BlackBench results for the SLC component in the Supplementary material.

5 Discussion

Kuro Siwo evaluation: Quantitative comparison of Kuro Siwo with other datasets is challenging, as most publicly available SAR-based datasets do not follow the same evaluation principles. These principles include testing on events absent from the training set and ensuring a diverse array of test events.

We identify MMFlood as the most fitting dataset for our comparison, offering 34 GRD test events with labels acquired from CEMS. The authors report a maximum of 66.52% mIoU solving the binary flood/no flood task, which is significantly lower than the one presented in BlackBench, where we solve a multi-class problem. This may be an indirect consequence of the problematic nature of CEMS labels as discussed in Sec. 3 and an indicator for the importance of accurate and cross verified ground truth labels. Another likely reason could be the oversight of the temporal dimension, as only post-event images are being used. Examining Tab. 2, we observe that the temporal aspect is crucial for semantic segmentation models, with most performing best when utilizing all available pre-event images. Conversely, incorporating DEM information offers negligible improvements. Even when

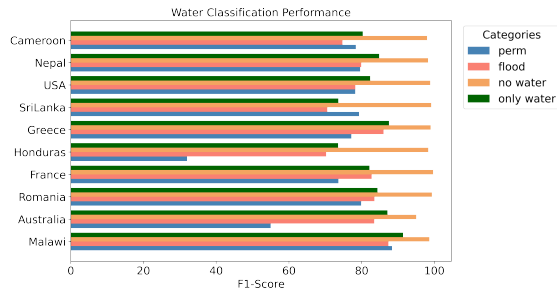


Figure 3: Per-event performance of the best model in BlackBench on the test set.

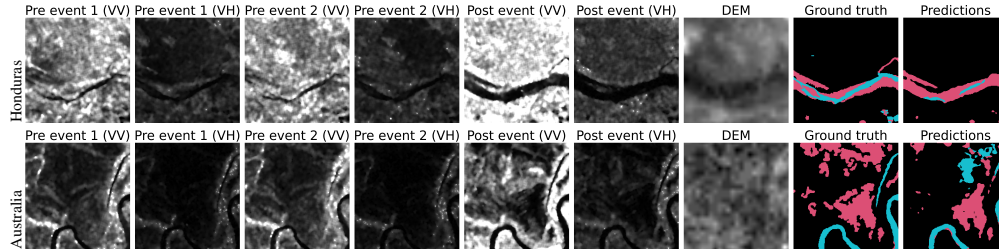


Figure 4: Qualitative evaluation of our best model in Honduras and Australia. Flood is marked in purple, permanent waters in cyan and non-water areas in black.

including DEM yields the best results for a model, the performance gains are marginal. Interestingly, we notice a consistent discrepancy across models in Tab. 2 between the reported metrics for permanent water bodies and the rest of the classes. We hypothesize that this behaviour stems from the inherent challenge of discerning permanent water bodies from flooded areas in specific locations, especially close to overflowed rivers and lakes.

This problem is magnified by the constant flow of water, resulting in small changes in the area it populates which in turn materializes with different signatures for each SAR timestep. This effect has a stronger presence in Fig. 3, where we present the per-event performance of the best model in BlackBench, i.e. UNet-ResNet50. Overall, we notice a stable performance despite the variable environmental conditions between events. However, performance in permanent waters detection drastically decreases for Honduras and Australia. We provide a qualitative examination of samples from these areas in Fig. 4. Indeed, we observe good detection of both flooded areas and permanent water bodies, however it is particularly challenging to accurately delineate their boundaries when they overlap.

Notably, FloodViT performs comparably with most models and surpasses all change detection methods despite having only a small decoder trained for the segmentation task. We did not observe additional benefits from fine-tuning FloodViT-FT. Further investigation on SSL methods for this task is left as future work.

SLC dataset: The inclusion of the unrefined SLC products paired with quality annotations at a global scale is an important aspect of Kuro Siwo. This component frees the end user of the task-specific preprocessing choices of the dataset creators, while enabling the investigation of important research questions such as the exploitation of the complex valued signal nature of SAR data. Our initial experiments (see Tab.2 in Supplementary material) suggest that DL models trained on SLC data are capable classifiers even on such unrefined data. In fact, a simple UNet with a ResNet18 backbone is able to achieve $\approx 79.94\%$ F-Score on the binary water detection task and $\approx 71.20\%$ and $\approx 76.76\%$ on the flood and permanent waters categories respectively. This is particularly promising since models in BlackBench are not tailored to the unique characteristics of SLC data. The thorough exploration of the complex information of SAR data is left as future work.

Limitations: Despite significant efforts to create a quality and diverse flood mapping dataset, approximately half of Kuro Siwo’s flood events are from Europe, with the rest distributed globally, indicating a need for more balanced spatial coverage. Furthermore, while Kuro Siwo can train models to map observed flood extents from SAR images, accurately capturing the actual maximum flood extent remains dependent on the revisit time of the Sentinel-1 mission. Finally, the inherent challenges associated with SAR data are a key limitation of Kuro Siwo. For example, speckle effect introduces granular noise that complicates the differentiation between flooded and non-flooded areas. Complex terrain and varying land cover types, such as forests, further complicate flood detection by affecting radar signal interaction. Variations in water surface roughness due to wind or the existence of vegetation can alter backscatter, making it difficult to consistently identify floodwaters. Detecting floods beneath dense vegetation is also challenging, as the S1 C-band radar signal may not penetrate sufficiently (as opposed to L-band SAR sensors) to reveal underlying water. Urban areas pose another difficulty, as radar signals often produce complex scattering effects (e.g. double-bounce reflections), making it difficult to distinguish between water and other surfaces, like wet roads or buildings.

Future research directions: Multispectral data, such as those provided by the Sentinel-2 constellation, can significantly aid flood mapping under cloud-free conditions since they provide a clearer view of the underlying waters compared to SAR. Incorporating multispectral imagery in Kuro Siwo

would require extensive photointerpretation, as acquisition timestamps between the satellites would possibly differ leading to discrepancies in detected flood events, given the short life cycle of flash floods. Nevertheless, the synergistic use of both datasets is a promising research direction, combining the precision of multispectral data with the all-weather resilience of SAR. Having Kuro Siwo as a publicly available resource with reliable SAR based annotations can provide the foundation for assembling such a multi-modal dataset.

Moreover, including a permanent water layer could be beneficial for discriminating between the two water classes. However, water bodies exhibit dynamic variable extents due to a variety of factors including meteorological conditions and environmental changes. Using a static water layer as input to the models could potentially impute noise and ultimately disrupt the learning process. Refining existing layers for each timestep in Kuro Siwo could prove counterintuitive in production as rapid flood mapping is of utmost importance. Further investigation on such auxiliary information is left as future work.

Finally, a related but fundamentally different topic than rapid flood mapping is flood forecasting. Kuro Siwo is focused on supporting emergency response activities within short time frames rather than long-term monitoring of water bodies for disaster resilience. While crucial, this task demands a distinct approach and additional data, such as local weather patterns, water storage capacity, soil data, and denser time series. Future research on this topic could strongly complement Kuro Siwo.

6 Conclusion

In this work, we release Kuro Siwo, a global, multi-temporal SAR dataset for flood mapping that includes both Level-1 GRD and SLC products. Kuro Siwo features manual annotations for 43 flood events worldwide, providing time series SAR data with dual polarization and elevation information. Alongside the curated dataset, we also release a large unlabeled dataset for large-scale self-supervised learning. Additionally, we introduce BlackBench, the first unified benchmark on Kuro Siwo, offering strong baselines for rapid flood mapping. We strongly believe that the release of Kuro Siwo will propel research in the crucial task of rapid flood mapping, potentially aiding in disaster response and relief management.

Acknowledgments and Disclosure of Funding

This work has received funding from the project ThinkingEarth (grant agreement No 101130544) and from the project MeDiTwin (grant agreement No 101159723) of the European Union’s Horizon Europe research and innovation programme.

References

- [1] Aparna, A., Sudha, N., et al. (2022). Sar-floodnet: A patch-based convolutional neural network for flood detection on sar images. *2022 International Conference on Applied Artificial Intelligence and Computing (ICAAIC)*, pages 195–200.
- [2] Asiyabi, R. M., Datcu, M., Anghel, A., and Nies, H. (2023). Complex-valued end-to-end deep network with coherency preservation for complex-valued sar data reconstruction and classification. *IEEE Transactions on Geoscience and Remote Sensing*, 61:1–17.
- [3] Bai, Y., Wu, W., Yang, Z., Yu, J., Zhao, B., Liu, X., Yang, H., Mas, E., and Koshimura, S. (2021). Enhancement of detecting permanent water and temporary water in flood disasters by fusing sentinel-1 and sentinel-2 imagery using deep learning algorithms: Demonstration of sen1floods11 benchmark datasets. *Remote Sensing*, 13(11):2220.
- [4] Bandara, W. G. C. and Patel, V. M. (2022). A transformer-based siamese network for change detection. In *IGARSS 2022 - 2022 IEEE International Geoscience and Remote Sensing Symposium*, pages 207–210.
- [5] Bates, P. D., Neal, J. C., Alsdorf, D., and Schumann, G. J.-P. (2014). Observing global surface water flood dynamics. *The Earth’s Hydrological Cycle*, pages 839–852.

- [6] Bevacqua, E., Vousedoukas, M. I., Zappa, G., Hodges, K., Shepherd, T. G., Maraun, D., Mentaschi, L., and Feyen, L. (2020). More meteorological events that drive compound coastal flooding are projected under climate change. *Communications Earth & Environment*, 1(1):47.
- [7] Böhm, V., Leong, W. J., Mahesh, R. B., Prapas, I., Nemni, E., Kalaitzis, F., Ganju, S., and Ramos-Pollan, R. (2022). Sar-based landslide classification pretraining leads to better segmentation. *arXiv preprint arXiv:2211.09927*.
- [8] Bonafilia, D., Tellman, B., Anderson, T., and Issenberg, E. (2020). Sen1floods11: A georeferenced dataset to train and test deep learning flood algorithms for sentinel-1. *Proceedings of the IEEE/CVF Conference on Computer Vision and Pattern Recognition Workshops*, pages 210–211.
- [9] Bountos, N. I., Papoutsis, I., Michail, D., Karavias, A., Elias, P., and Parcharidis, I. (2022). Hephaestus: A large scale multitask dataset towards insar understanding. *Proceedings of the IEEE/CVF Conference on Computer Vision and Pattern Recognition*, pages 1453–1462.
- [10] Brivio, P., Colombo, R., Maggi, M., and Tomasoni, R. (2002). Integration of remote sensing data and gis for accurate mapping of flooded areas. *International Journal of Remote Sensing*, 23(3):429–441.
- [11] Brouwer, R., Akter, S., Brander, L., and Haque, E. (2007). Socioeconomic vulnerability and adaptation to environmental risk: a case study of climate change and flooding in bangladesh. *Risk Analysis: An International Journal*, 27(2):313–326.
- [12] Chen, L.-C., Papandreou, G., Schroff, F., and Adam, H. (2017). Rethinking atrous convolution for semantic image segmentation. *arXiv preprint arXiv:1706.05587*.
- [13] Chouhan, A., Chutia, D., and Aggarwal, S. P. (2023). Attentive decoder network for flood analysis using sentinel 1 images. *2023 International Conference on Communication, Circuits, and Systems (IC3S)*, pages 1–5.
- [14] Cian, F., Marconcini, M., and Ceccato, P. (2018). Normalized difference flood index for rapid flood mapping: Taking advantage of eo big data. *Remote Sensing of Environment*, 209:712–730.
- [15] Contributors, M. (2020). MMSegmentation: Openmmlab semantic segmentation toolbox and benchmark. <https://github.com/open-mmlab/mms Segmentation>.
- [16] Cumming, I. G. and Wong, F. H. (2005). Digital processing of synthetic aperture radar data. *Artech house*, 1(3):108–110.
- [17] Daudt, R. C., Le Saux, B., and Boulch, A. (2018). Fully convolutional siamese networks for change detection. In *2018 25th IEEE international conference on image processing (ICIP)*, pages 4063–4067. IEEE.
- [18] Deng, J., Dong, W., Socher, R., Li, L.-J., Li, K., and Fei-Fei, L. (2009). Imagenet: A large-scale hierarchical image database. *2009 IEEE conference on computer vision and pattern recognition*, pages 248–255.
- [19] Domeneghetti, A., Schumann, G. J.-P., and Tarpanelli, A. (2019). Preface: remote sensing for flood mapping and monitoring of flood dynamics. *Remote Sensing*, 11(8):943.
- [20] Dong, Z., Liang, Z., Wang, G., Amankwah, S. O. Y., Feng, D., Wei, X., and Duan, Z. (2023). Mapping inundation extents in Poyang Lake area using Sentinel-1 data and transformer-based change detection method. *Journal of Hydrology*, 620:129455.
- [21] Dosovitskiy, A., Beyer, L., Kolesnikov, A., Weissenborn, D., Zhai, X., Unterthiner, T., Dehghani, M., Minderer, M., Heigold, G., Gelly, S., et al. (2020). An image is worth 16x16 words: Transformers for image recognition at scale. *arXiv preprint arXiv:2010.11929*.
- [22] Drakonakis, G. I., Tsagakatakis, G., Fotiadou, K., and Tsakalides, P. (2022). Ombri-net—supervised flood mapping via convolutional neural networks using multitemporal sentinel-1 and sentinel-2 data fusion. *IEEE Journal of Selected Topics in Applied Earth Observations and Remote Sensing*, 15:2341–2356.

- [23] Eini, M., Kaboli, H. S., Rashidian, M., and Hedayat, H. (2020). Hazard and vulnerability in urban flood risk mapping: Machine learning techniques and considering the role of urban districts. *International Journal of Disaster Risk Reduction*, 50:101687.
- [24] Fang, S., Li, K., Shao, J., and Li, Z. (2021). Snunet-cd: A densely connected siamese network for change detection of vhr images. *IEEE Geoscience and Remote Sensing Letters*, 19:1–5.
- [25] Filippini, F. (2019). Sentinel-1 grd preprocessing workflow. *International Electronic Conference on Remote Sensing*, page 11.
- [26] Garg, S., Feinstein, B., Timnat, S., Batchu, V., Dror, G., Rosenthal, A. G., and Gulshan, V. (2023). Cross-modal distillation for flood extent mapping. *Environmental Data Science*, 2:e37.
- [27] Gong, M., Yang, H., and Zhang, P. (2017). Feature learning and change feature classification based on deep learning for ternary change detection in sar images. *ISPRS Journal of Photogrammetry and Remote Sensing*, 129:212–225.
- [28] Graham-McLay, C. (2023). Auckland floods: city begins clean-up after ‘biggest climate event’ in New Zealand’s history. *The Guardian*. <https://www.theguardian.com/world/2023/feb/01/auckland-floods-biggest-climate-event-new-zealand-history-flooding> [Accessed: 2023-02-01].
- [29] He, K., Chen, X., Xie, S., Li, Y., Dollár, P., and Girshick, R. (2022). Masked autoencoders are scalable vision learners. *Proceedings of the IEEE/CVF conference on computer vision and pattern recognition*, pages 16000–16009.
- [30] He, K., Zhang, X., Ren, S., and Sun, J. (2016). Deep residual learning for image recognition. *Proceedings of the IEEE conference on computer vision and pattern recognition*, pages 770–778.
- [31] He, X., Zhang, S., Xue, B., Zhao, T., and Wu, T. (2023). Cross-modal change detection flood extraction based on convolutional neural network. *International Journal of Applied Earth Observation and Geoinformation*, 117:103197.
- [32] Henry, J.-B., Chastanet, P., Fellah, K., and Desnos, Y.-L. (2006). Envisat multi-polarized asar data for flood mapping. *International Journal of Remote Sensing*, 27(10):1921–1929.
- [33] Islam, K. A., Uddin, M. S., Kwan, C., and Li, J. (2020). Flood detection using multi-modal and multi-temporal images: A comparative study. *Remote Sensing*, 12(15):2455.
- [34] Ji, L., Zhao, Z., Huo, W., Zhao, J., and Gao, R. (2022). Evaluation of several fully convolutional network in sar image change detection. *ISPRS Annals of the Photogrammetry, Remote Sensing and Spatial Information Sciences*, X-3/W1-2022:61–68.
- [35] Jiang, X., Liang, S., He, X., Ziegler, A. D., Lin, P., Pan, M., Wang, D., Zou, J., Hao, D., Mao, G., Zeng, Y., Yin, J., Feng, L., Miao, C., Wood, E. F., and Zeng, Z. (2021). Rapid and large-scale mapping of flood inundation via integrating spaceborne synthetic aperture radar imagery with unsupervised deep learning. *ISPRS Journal of Photogrammetry and Remote Sensing*, 178:36–50.
- [36] Jongman, B., Wagemaker, J., Revilla Romero, B., and Coughlan de Perez, E. (2015). Early flood detection for rapid humanitarian response: harnessing near real-time satellite and twitter signals. *ISPRS International Journal of Geo-Information*, 4(4):2246–2266.
- [37] Jonkman, S. N. (2005). Global perspectives on loss of human life caused by floods. *Natural hazards*, 34(2):151–175.
- [38] Kang, W., Xiang, Y., Wang, F., Wan, L., and You, H. (2018). Flood detection in gaofen-3 sar images via fully convolutional networks. *Sensors*, 18(9):2915.
- [39] Katiyar, V., Tamkuan, N., and Nagai, M. (2021). Near-real-time flood mapping using off-the-shelf models with sar imagery and deep learning. *Remote Sensing*, 13(12):2334.
- [40] Kirillov, A., Mintun, E., Ravi, N., Mao, H., Rolland, C., Gustafson, L., Xiao, T., Whitehead, S., Berg, A. C., Lo, W.-Y., et al. (2023). Segment anything. In *Proceedings of the IEEE/CVF International Conference on Computer Vision*, pages 4015–4026.

- [41] Kondylatos, S., Prapas, I., Camps-Valls, G., and Papoutsis, I. (2023). Mesogeos: A multi-purpose dataset for data-driven wildfire modeling in the mediterranean. In *Advances in Neural Information Processing Systems*, volume 36, pages 50661–50676. Curran Associates, Inc.
- [42] Kreibich, H., Bubeck, P., Van Vliet, M., and De Moel, H. (2015). A review of damage-reducing measures to manage fluvial flood risks in a changing climate. *Mitigation and adaptation strategies for global change*, 20:967–989.
- [43] Lee, J.-S., Jurkevich, L., Dewaele, P., Wambacq, P., and Oosterlinck, A. (1994). Speckle filtering of synthetic aperture radar images: A review. *Remote sensing reviews*, 8(4):313–340.
- [44] Li, B., Liu, B., Huang, L., Guo, W., Zhang, Z., and Yu, W. (2017). Opensarship 2.0: A large-volume dataset for deeper interpretation of ship targets in sentinel-1 imagery. In *2017 SAR in Big Data Era: Models, Methods and Applications (BIGSAR DATA)*, pages 1–5. IEEE.
- [45] Liu, B., Li, X., and Zheng, G. (2019). Coastal inundation mapping from bitemporal and dual-polarization sar imagery based on deep convolutional neural networks. *Journal of Geophysical Research: Oceans*, 124(12):9101–9113.
- [46] Liu, Q., Ren, K., Meng, X., and Shao, F. (2023). Domain adaptive cross-reconstruction for change detection of heterogeneous remote sensing images via a feedback guidance mechanism. *IEEE Transactions on Geoscience and Remote Sensing*, 61:1–16.
- [47] Liu, Z., Lin, Y., Cao, Y., Hu, H., Wei, Y., Zhang, Z., Lin, S., and Guo, B. (2021). Swin transformer: Hierarchical vision transformer using shifted windows. *Proceedings of the IEEE/CVF international conference on computer vision*, pages 10012–10022.
- [48] Liu, Z., Mao, H., Wu, C.-Y., Feichtenhofer, C., Darrell, T., and Xie, S. (2022). A convnet for the 2020s. *Proceedings of the IEEE/CVF Conference on Computer Vision and Pattern Recognition*, pages 11976–11986.
- [49] Martinez, J.-M. and Le Toan, T. (2007). Mapping of flood dynamics and spatial distribution of vegetation in the amazon floodplain using multitemporal sar data. *Remote sensing of Environment*, 108(3):209–223.
- [50] Martinez-Villalobos, C. and Neelin, J. D. (2023). Regionally high risk increase for precipitation extreme events under global warming. *Scientific Reports*, 13(1):5579.
- [51] Mateo-Garcia, G., Veitch-Michaelis, J., Smith, L., Oprea, S. V., Schumann, G., Gal, Y., Baydin, A. G., and Backes, D. (2021). Towards global flood mapping onboard low cost satellites with machine learning. *Scientific Reports*, 11(1):7249.
- [52] Matheswaran, K., Alahacoon, N., Pandey, R., and Amarnath, G. (2019). Flood risk assessment in south asia to prioritize flood index insurance applications in bihar, india. *Geomatics, Natural Hazards and Risk*, 10(1):26–48.
- [53] Membele, G. M., Naidu, M., and Mutanga, O. (2022). Examining flood vulnerability mapping approaches in developing countries: A scoping review. *International Journal of Disaster Risk Reduction*, 69:102766.
- [54] Merz, B., Blöschl, G., Vorogushyn, S., Dottori, F., Aerts, J. C., Bates, P., Bertola, M., Kemter, M., Kreibich, H., Lall, U., et al. (2021). Causes, impacts and patterns of disastrous river floods. *Nature Reviews Earth & Environment*, 2(9):592–609.
- [55] Mokrech, M., Kebede, A., Nicholls, R., Wimmer, F., and Feyen, L. (2015). An integrated approach for assessing flood impacts due to future climate and socio-economic conditions and the scope of adaptation in europe. *Climatic Change*, 128:245–260.
- [56] Montello, F., Arnaudo, E., and Rossi, C. (2022). Mmflood: A multimodal dataset for flood delineation from satellite imagery. *IEEE Access*, 10:96774–96787.
- [57] Monti-Guarnieri, A. V., Brovelli, M. A., Manzoni, M., Mariotti d’Alessandro, M., Molinari, M. E., and Oxoli, D. (2018). Coherent change detection for multipass sar. *IEEE Transactions on Geoscience and Remote Sensing*, 56(11):6811–6822.

- [58] Muñoz, D. F., Muñoz, P., Moftakhari, H., and Moradkhani, H. (2021). From local to regional compound flood mapping with deep learning and data fusion techniques. *Science of The Total Environment*, 782:146927.
- [59] NASA-IMPACT (2021). *ETCI 2021 Competition on Flood Detection*. <https://nasa-impact.github.io/etci2021/> [Accessed: 2024-05-30].
- [60] Nemni, E., Bullock, J., Belabbes, S., and Bromley, L. (2020). Fully Convolutional Neural Network for Rapid Flood Segmentation in Synthetic Aperture Radar Imagery. *Remote Sensing*, 12(16):2532.
- [61] Nkwunonwo, U., Whitworth, M., and Baily, B. (2020). A review of the current status of flood modelling for urban flood risk management in the developing countries. *Scientific African*, 7:e00269.
- [62] Papoutsis, I., Bountos, N. I., Zavras, A., Michail, D., and Tryfonopoulos, C. (2023). Benchmarking and scaling of deep learning models for land cover image classification. *ISPRS Journal of Photogrammetry and Remote Sensing*, 195:250–268.
- [63] Pulvirenti, L., Chini, M., Pierdicca, N., and Boni, G. (2016). Use of sar data for detecting floodwater in urban and agricultural areas: The role of the interferometric coherence. *IEEE Transactions on Geoscience and Remote Sensing*, 54(3):1532–1544.
- [64] Rahnemoonfar, M., Chowdhury, T., Sarkar, A., Varshney, D., Yari, M., and Murphy, R. R. (2021). Floodnet: A high resolution aerial imagery dataset for post flood scene understanding. *IEEE Access*, 9:89644–89654.
- [65] Rambour, C., Audebert, N., Koeniguer, E., Le Saux, B., Crucianu, M., and Datcu, M. (2020). Flood detection in time series of optical and sar images. *The International Archives of the Photogrammetry, Remote Sensing and Spatial Information Sciences*, XLIII-B2-2020:1343–1346.
- [66] Raymond, C., Horton, R. M., Zscheischler, J., Martius, O., AghaKouchak, A., Balch, J., Bowen, S. G., Camargo, S. J., Hess, J., Kornhuber, K., et al. (2020). Understanding and managing connected extreme events. *Nature climate change*, 10(7):611–621.
- [67] Rentschler, J., Salhab, M., and Jafino, B. A. (2022). Flood exposure and poverty in 188 countries. *Nature Communications*, 13(1):3527.
- [68] Rodell, M. and Li, B. (2023). Changing intensity of hydroclimatic extreme events revealed by grace and grace-fo. *Nature Water*, 1(3):241–248.
- [69] Ronneberger, O., Fischer, P., and Brox, T. (2015). U-net: Convolutional networks for biomedical image segmentation. *Medical Image Computing and Computer-Assisted Intervention–MICCAI 2015: 18th International Conference, Munich, Germany, October 5-9, 2015, Proceedings, Part III 18*, pages 234–241.
- [70] Rufat, S., Tate, E., Burton, C. G., and Maroof, A. S. (2015). Social vulnerability to floods: Review of case studies and implications for measurement. *International journal of disaster risk reduction*, 14:470–486.
- [71] Saleh, T., Weng, X., Holail, S., Hao, C., and Xia, G.-S. (2024). Dam-net: Flood detection from sar imagery using differential attention metric-based vision transformers. *ISPRS Journal of Photogrammetry and Remote Sensing*, 212:440–453.
- [72] Seneviratne, S. I., Zhang, X., Adnan, M., Badi, W., Dereczynski, C., Di Luca, A., Ghosh, S., Iskander, I., Kossin, J., Lewis, S., et al. (2021). Weather and climate extreme events in a changing climate (chapter 11). In *IPCC 2021: Climate Change 2021: The Physical Science Basis. Contribution of Working Group I to the Sixth Assessment Report of the Intergovernmental Panel on Climate Change*, pages 1513–1766. Cambridge University Press.
- [73] Shi, X., Chen, Z., Wang, H., Yeung, D.-Y., Wong, W.-K., and Woo, W.-c. (2015). Convolutional lstm network: A machine learning approach for precipitation nowcasting. *Advances in neural information processing systems*, 28.

- [74] Sumbul, G., Charfuelan, M., Demir, B., and Markl, V. (2019). Bigearthnet: A large-scale benchmark archive for remote sensing image understanding. *IGARSS 2019-2019 IEEE International Geoscience and Remote Sensing Symposium*, pages 5901–5904.
- [75] Sykas, D., Sdraka, M., Zografakis, D., and Papoutsis, I. (2022). A sentinel-2 multiyear, multicountry benchmark dataset for crop classification and segmentation with deep learning. *IEEE Journal of Selected Topics in Applied Earth Observations and Remote Sensing*, 15:3323–3339.
- [76] Tellman, B., Lall, U., Islam, A. S., and Bhuyan, M. A. (2022). Regional index insurance using satellite-based fractional flooded area. *Earth's Future*, 10(3):e2021EF002418.
- [77] Tellman, B., Sullivan, J., Kuhn, C., Kettner, A., Doyle, C., Brakenridge, G., Erickson, T., and Slayback, D. (2021). Satellite imaging reveals increased proportion of population exposed to floods. *Nature*, 596(7870):80–86.
- [78] Thomas, M., Tellman, E., Osgood, D. E., DeVries, B., Islam, A. S., Steckler, M. S., Goodman, M., and Billah, M. (2023). A framework to assess remote sensing algorithms for satellite-based flood index insurance. *IEEE Journal of Selected Topics in Applied Earth Observations and Remote Sensing*, 16:2589–2604.
- [79] Twele, A., Cao, W., Plank, S., and Martinis, S. (2016). Sentinel-1-based flood mapping: a fully automated processing chain. *International Journal of Remote Sensing*, 37(13):2990–3004.
- [80] Uddin, K. and Matin, M. A. (2021). Potential flood hazard zonation and flood shelter suitability mapping for disaster risk mitigation in bangladesh using geospatial technology. *Progress in disaster science*, 11:100185.
- [81] Unicef (2022). Devastating floods in Pakistan. <https://www.unicef.org/emergencies/devastating-floods-pakistan-2022> [Accessed: 2023-02-01].
- [82] Waseem, H. B. and Rana, I. A. (2023). Floods in pakistan: A state-of-the-art review. *Natural Hazards Research*, 3(3):359–373.
- [83] World-Bank (2022). Pakistan: Flood Damages and Economic Losses Over USD 30 billion and Reconstruction Needs Over USD 16 billion - New Assessment. https://www.worldbank.org/en/news/PRESS_RELEASE_NO:SAR/2022 [Accessed: 2023-02-01].
- [84] Wu, C., Yang, X., and Wang, J. (2019). Flood Detection in Sar Images Based on Multi-Depth Flood Detection Convolutional Neural Network. *2019 6th Asia-Pacific Conference on Synthetic Aperture Radar (APSAR)*, pages 1–6.
- [85] Wu, H., Song, H., Huang, J., Zhong, H., Zhan, R., Teng, X., Qiu, Z., He, M., and Cao, J. (2022). Flood detection in dual-polarization sar images based on multi-scale deeplab model. *Remote Sensing*, 14(20):5181.
- [86] Wu, X., Zhang, Z., Xiong, S., Zhang, W., Tang, J., Li, Z., An, B., and Li, R. (2023). A Near-Real-Time Flood Detection Method Based on Deep Learning and SAR Images. *Remote Sensing*, 15(8):2046.
- [87] Xiao, T., Liu, Y., Zhou, B., Jiang, Y., and Sun, J. (2018). Unified perceptual parsing for scene understanding. *Proceedings of the European conference on computer vision (ECCV)*, pages 418–434.
- [88] Yadav, R., Nascetti, A., Azizpour, H., and Ban, Y. (2022). Unsupervised Flood Detection on SAR Time Series. arXiv:2212.03675 [cs].
- [89] Yang, Q., Shen, X., Anagnostou, E. N., Mo, C., Eggleston, J. R., and Kettner, A. J. (2021). A high-resolution flood inundation archive (2016–the present) from sentinel-1 sar imagery over conus. *Bulletin of the American Meteorological Society*, pages 1–40.
- [90] Zhang, H., Lin, Z., Gao, F., Dong, J., Du, Q., and Li, H.-C. (2023a). Convolution and attention mixer for synthetic aperture radar image change detection. *IEEE Geoscience and Remote Sensing Letters*, 20:1–5.

- [91] Zhang, Y., Liu, P., Chen, L., Xu, M., Guo, X., and Zhao, L. (2023b). A new multi-source remote sensing image sample dataset with high resolution for flood area extraction: Gf-floodnet. *International Journal of Digital Earth*, 16(1):2522–2554.
- [92] Zhang, Y., Liu, P., Chen, L., Xu, M., Guo, X., and Zhao, L. (2023c). A new multi-source remote sensing image sample dataset with high resolution for flood area extraction: GF-FloodNet. *International Journal of Digital Earth*, 16(1):2522–2554.
- [93] Zhao, B., Sui, H., and Liu, J. (2023). Siam-DWENet: Flood inundation detection for SAR imagery using a cross-task transfer siamese network. *International Journal of Applied Earth Observation and Geoinformation*, 116:103132.
- [94] Zhou, Z., Rahman Siddiquee, M. M., Tajbakhsh, N., and Liang, J. (2018). Unet++: A nested u-net architecture for medical image segmentation. *Deep Learning in Medical Image Analysis and Multimodal Learning for Clinical Decision Support: 4th International Workshop, DLMIA 2018, and 8th International Workshop, ML-CDS 2018, Held in Conjunction with MICCAI 2018, Granada, Spain, September 20, 2018, Proceedings 4*, pages 3–11.
- [95] Zuhlke, M., Fomferra, N., Brockmann, C., Peters, M., Veci, L., Malik, J., and Regner, P. (2015). Snap (sentinel application platform) and the esa sentinel 3 toolbox. *Sentinel-3 for Science Workshop*, 734:21.

Supplemental material

1 Dataset

The total size of the compressed dataset is ≈ 1.33 TB, with the GRD component (including the DEMs and metadata) taking ≈ 705.8 GB and the SLC ≈ 492.6 GB.

All code and data will be maintained at the project’s repo.

2 Evaluation on a new, unseen event

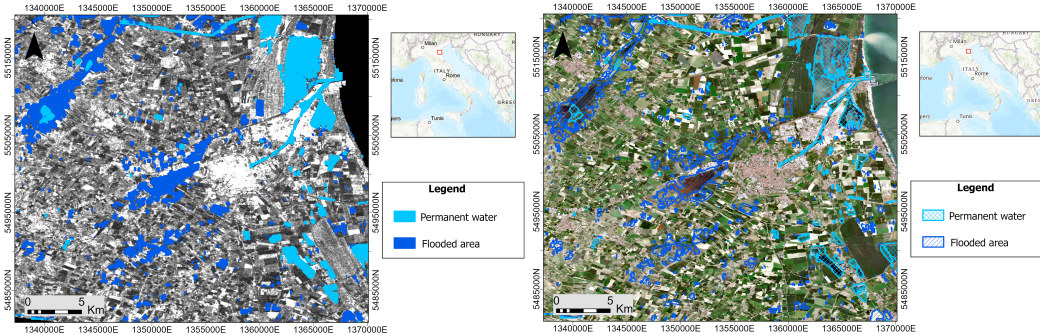


Figure 5: Predictions of the flood and permanent water extent using our best model, i.e. UNet-ResNet50, on Emilia-Romagna floods in May 2023. On the left hand side we present the post-event SAR image used for the prediction, captured in 22/05/2023, while on the right hand side the respective Sentinel-2 RGB image captured in 23/05/2023 (one day later).

In Fig. 5 we assess the performance of our best model, i.e. UNet-ResNet50, on the recent floods of Emilia-Romagna, Italy, which took place on May 2023. Our predictions were based on a post-event SAR image acquired on 22/05/2023, and two pre-event SAR images from 10/05/2023 and 28/04/2023. On the right hand side of Fig. 5 we overlay our predictions with a Sentinel-2 RGB image captured on 23/05/2023 for better inspection of the annotated areas. Examining both derived maps we clearly see the capacity of the proposed model, showcasing the quality of Kuro Siwo. Our model manages to uncover all major water bodies, such as the rivers and ponds in the Pialassa della Baiona, as well as flooded regions of diverse sizes. Given that BlackBench presents baseline models, the performance of future task-specific methods may potentially surpass the baselines offered in this work.

3 Additional results

Fig. 6 showcases representative samples from the Kuro Siwo GRD dataset, providing a closer examination of flood events spanning a diverse set of countries. The predictions come from the best performing model in BlackBench, i.e UNet-ResNet50. The results underscore the significance of leveraging both polarization bands (VV and VH) for an accurate evaluation of the influence of the underlying land cover. While the VV band is effective in detecting the majority of flooded areas, the post-flood VV imagery may also include some bright regions in flooded areas that might be mistaken for dry land. These areas are refined and clarified by incorporating the VH band, which exhibits a more uniform dark region with smaller bright patches. For example, the flooded area in Fig. 6e is more concretely depicted in the VH band with stronger backscatter in the regions farthest from the river which also present a challenge to our model.

On the contrary, Fig. 6b, Fig. 6g and Fig. 6e feature specific dark regions in the pre-flood imagery that are not labeled as water bodies in the annotation. These areas may correspond to isolated pixels experiencing the speckle effects or to crop parcels or vegetated areas with varying moisture content, that are in different phenological states compared to neighboring regions. In general, the model manages to successfully capture the outline of most water elements, albeit often missing narrow rivers, which is a rather difficult task considering the dynamic nature of water flow and the changes of river width over time.

Furthermore, Fig. 6c and Fig. 6d present instances of river overflow. The Kuro Siwo annotation precisely delineates the initial river shape as inferred by the two pre-event captions, along with the flooded river banks marked in purple. In Fig. 6d, the Unet-ResNet50 achieves high accuracy in both permanent waters and flood, whereas in Fig. 6c it seems to miss the exact shape of the river in which is depicted in a more solid black region in the VH band. Furthermore, the overflowed river banks present a significant challenge for the model which is constantly confused between the two water classes.

Finally, Fig. 6h presents a particularly challenging sample, wherein the small reservoir of permanent water in the upper-left of the patch is difficult to detect due to the strong presence of SAR speckle noise.

4 Annotation process

The outlined annotation process unfolds in distinct phases: initially, we establish the entire procedure by defining the annotation categories, i.e. “Permanent Waters”, “Floods” and “No Water”. We extract the corresponding photointerpretation keys, set the annotation scale to 1:1000, and establish criteria for flagging artifacts in the input data. Next, we partition the 43 flood events into five segments. A team of five SAR experts undertook the annotation process, with each member assigned to annotate one part and quality-check the annotations of another team member. The supervision of this process was overseen by a senior remote sensing scientist. Regular group meetings were conducted to address and resolve any potential discrepancies between the primary annotator and the responsible for the quality check.

5 Training setup

In Table 4 we report the training hyperparameters for each model in BlackBench. All SAR images were clipped at a max value of 0.15 and normalized to 0 mean and 1 standard deviation. At training time we skip samples that do not contain water (regardless of the class). We test on all available samples of the test areas. All models utilize the cross-entropy loss function, apart from SNUNet-CD that employs a compound loss consisting of cross-entropy and Dice loss, in line with the original publication.

6 SLC benchmark

In Table 3 we present the BlackBench results for the SLC component of Kuro Siwo.

7 Computational resources

All experiments were conducted on a single NVIDIA GeForce RTX 3090 Ti.

8 Intended uses

Kuro Siwo is designed to address two primary objectives: a) overcoming the lack of large, meticulously annotated datasets for flash flood mapping and b) promoting the development of deep learning methods that utilize both phase and amplitude information, without restrictive preprocessing choices. The intended uses of Kuro Siwo are thus, a) the development of robust and accurate flash flood mapping methods, which could potentially be applied in operational settings, and b) research in the direct exploitation of complex SAR data.

9 License

The authors state that they bear all responsibility in case of any rights violation. The Kuro Siwo dataset as well as BlackBench are released under the MIT License.⁴

⁴<https://opensource.org/license/mit>

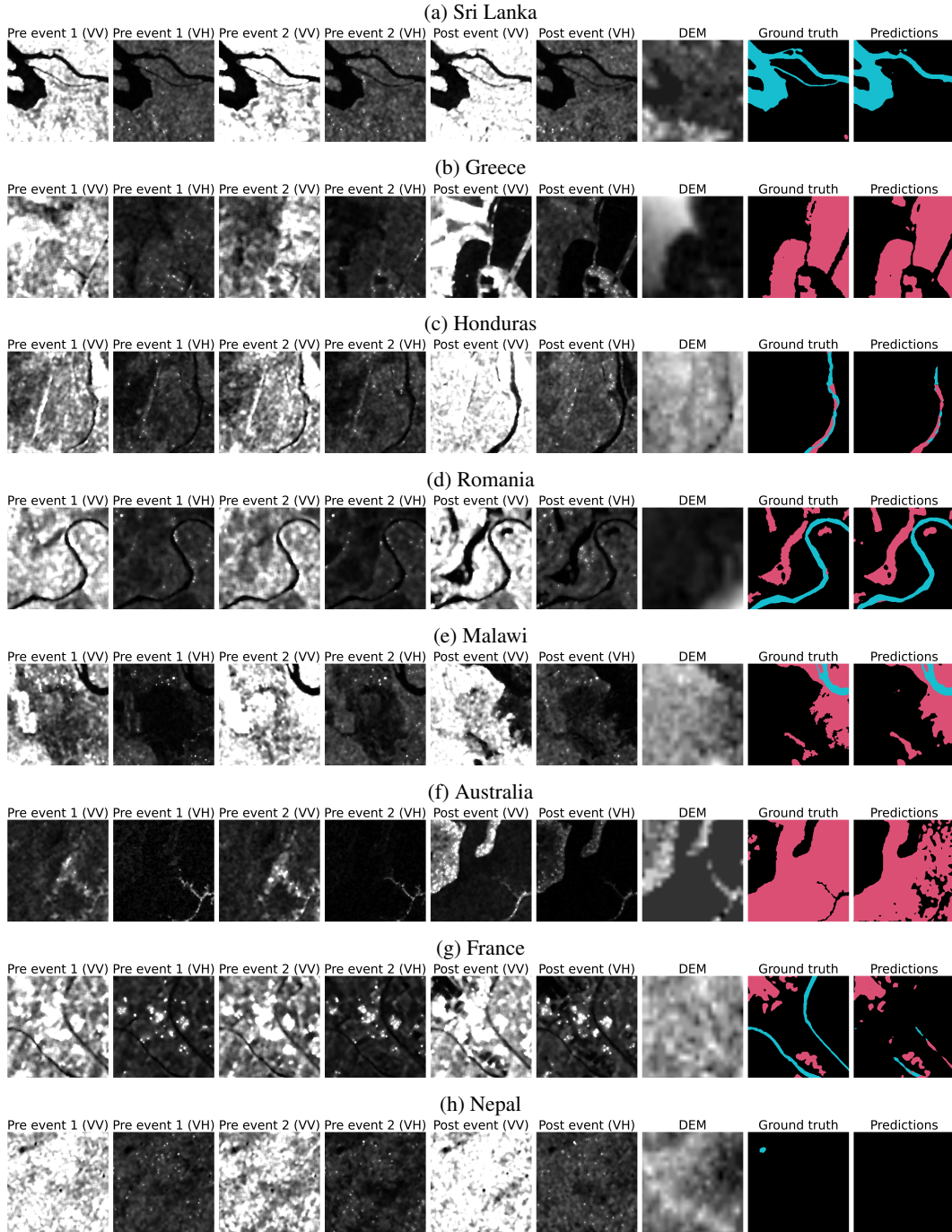


Figure 6: Kuro Siwo GRD samples. Flood is marked in purple, permanent waters in cyan and non-water areas in black. The predictions come from the best performing model in BlackBench, i.e UNet-ResNet50.

10 Maintenance plan

The main hosting platform of Kuro Siwo and BlackBench is GitHub and the authors guarantee access to the main code, as well as maintenance and issue tracking. Due to their seer size, data are hosted at a major cloud storage provider, ensuring seamless availability and adequate download speeds.

Table 3: This table presents the best performing setting for each architecture for the SLC component, in regards to the time series length as well as the utilization of elevation information. “No water”, “permanent water”, “flood” and “water” classes are represented by NW, PW, F and W respectively. Best values are marked in **bold**, second best are underlined.

Model	Caps.	DEM	Slope	F1-NW(%)	F1-PW(%)	F1-F(%)	mIOU(%)	F1-W(%)
UNet-ResNet18	3	-	✓	97.88	76.76	71.20	71.14	79.94
UNet-ResNet50	3	-	✓	97.68	78.76	68.91	71.00	78.10
UNet-ResNet101	3	-	✓	97.68	76.64	69.74	70.38	77.81
DeepLab-ResNet18	3	-	✓	97.63	74.21	69.15	69.08	<u>78.51</u>
DeepLab-ResNet50	2	-	✓	97.63	76.57	66.20	68.96	77.10
DeepLab-ResNet101	3	-	-	97.63	74.92	69.72	69.60	77.13
UPerNet-SwinS	3	-	-	97.71	79.48	70.39	71.93	78.17
UPerNet-SwinB	3	-	-	97.63	<u>79.16</u>	70.25	<u>71.68</u>	77.23
UPerNet-ConvnextS	3	-	-	97.64	<u>78.93</u>	69.33	71.22	77.45
UPerNet-ConvnextB	3	-	-	97.71	78.79	69.70	71.34	77.51
FloodViT	3	-	-	97.32	60.03	56.87	59.13	69.76
FloodViT-FT	3	-	-	96.84	51.23	57.62	56.26	61.43
FC-EF-Diff	2	✓	-	97.53	70.51	69.13	67.49	75.97
FC-EF-Conc	2	-	-	97.72	71.92	68.78	68.03	77.3
SNUNet-CD	2	-	✓	97.65	75.31	68.82	69.42	77.99
Changeformer	2	✓	-	97.61	69.31	69.34	67.14	75.87
ConvLSTM	3	-	-	<u>97.76</u>	78.16	<u>70.58</u>	71.44	78.0

Table 4: The training hyperparameters used in BlackBench. LR stands for learning rate and SGD for Stochastic Gradient Descent.

Model	Optimizer	LR	LR scheduling	Weight decay	# epochs
UNet-ResNet18	Adam	1e-3	Cosine	-	20
UNet-ResNet50	Adam	1e-3	Cosine	-	20
UNet-ResNet101	Adam	1e-3	Cosine	-	20
DeepLab-ResNet18	Adam	1e-3	Cosine	-	20
DeepLab-ResNet50	Adam	1e-3	Cosine	-	20
DeepLab-ResNet101	Adam	1e-3	Cosine	-	20
UPerNet-SwinS	Adam	1e-4	-	1e-4	20
UPerNet-SwinB	Adam	1e-4	-	1e-4	20
UPerNet-ConvnextS	Adam	1e-4	-	1e-4	20
UPerNet-ConvnextB	Adam	1e-4	-	1e-4	20
FloodViT	Adam	1e-3	Cosine	1e-5	20
FloodViT-FT	Adam	1e-4	Cosine	1e-3	20
FC-EF-Diff	Adam	1e-5	-	-	150
FC-EF-Conc	Adam	1e-5	-	-	150
SNUNet-CD	Adam	1e-5	-	-	150
Changeformer	SGD	6e-4	Linear	1e-5	150
ConvLSTM	Adam	1e-3	-	-	150